Gain bandwidth characterization of surface-emitting quantum well laser gain structures for femtosecond operation

Barnes, M. E.; Mihoubi, Z.; Wilcox, K. G.; Quarterman, A. H.; Farrer, I.; Ritchie, D. A.

Published in:
Optics Express

DOI:
10.1364/OE.18.021330

Publication date:
2010

Document Version
Publisher's PDF, also known as Version of record

Gain bandwidth characterization of surface-emitting quantum well laser gain structures for femtosecond operation

M. E. Barnes,[1] Z. Mihoubi,[1] K. G. Wilcox,[1] A. H. Quarterman,[1] I. Farrer,[2] D. A. Ritchie,[2] A. Garnache,[3] S. Hoogland,[4] and V. Apostolopoulos,[1] and A. C. Tropper[1,*]

[1]*School of Physics and Astronomy, University of Southampton, Southampton SO17 1BJ, UK*
[2]*Department of Physics, University of Cambridge, JJ Thomson Avenue, Cambridge, CB3 0HE, UK*
[3]*Institut d'Electronique de Sud, CNRS UMR5214, Université Montpellier 2, France*
[4]*University of Toronto M5S 3G4, Ontario, Canada*
**act@phys.soton.ac.uk*

Abstract: We present a method to experimentally characterize the gain filter and calculate a corresponding parabolic gain bandwidth of lasers that are described by "class A" dynamics by solving the master equation of spectral condensation for Gaussian spectra. We experimentally determine the gain filter, with an equivalent parabolic gain bandwidth of up to 51 nm, for broad-band InGaAs/GaAs quantum well gain surface-emitting semiconductor laser structures capable of producing pulses down to 60 fs width when mode-locked with an optical Stark saturable absorber mirror.

OCIS codes: 140.7090 Ultrafast lasers; 140.7260 Vertical cavity surface emitting lasers; 140.3430 Laser theory.

References and links

1. A. C. Tropper, H. D. Foreman, A. Garnache, K. G. Wilcox, and S. H. Hoogland, "Vertical-external-cavity semiconductor lasers," J. Phys. D Appl. Phys. **37**(9), R75–R85 (2004).
2. U. Keller, and A. C. Tropper, "Passively modelocked surface-emitting semiconductor lasers," Phys. Rep. **429**(2), 67–120 (2006).
3. P. Klopp, U. Griebner, M. Zorn, A. Klehr, A. Liero, M. Weyers, and G. Erbert, "Mode-locked InGaAs-AlGaAs disk laser generating sub-200-fs pulses, pulse picking and amplification by a tapered diode amplifier," Opt. Express **17**(13), 10820–10834 (2009).
4. H. A. Haus, "Theory of mode-locking with a fast saturable absorber," J. Appl. Phys. **46**(7), 3049–3058 (1975).
5. Z. Mihoubi, G. J. Daniell, K. G. Wilcox, and A. C. Tropper, "Numerical model of the optical Stark effect as a mode-locking mechanism for femtosecond vertical-external-cavity surface-emitting semiconductor lasers," in *CLEO/QELS'08* (San Jose CA, 2008).
6. A. Garnache, S. Hoogland, A. Tropper, I. Sagnes, G. Saint-Girons, and J. Roberts, "Sub-500-fs soliton-like pulse in a passively mode-locked broadband surface-emitting laser with 100 mW average power," Appl. Phys. Lett. **80**(21), 3892–3894 (2002).
7. K. G. Wilcox, Z. Mihoubi, G. J. Daniell, S. Elsmere, A. Quarterman, I. Farrer, D. A. Ritchie, and A. Tropper, "Ultrafast optical Stark mode-locked semiconductor laser," Opt. Lett. **33**(23), 2797–2799 (2008).
8. S. Hoogland, A. Garnache, I. Sagnes, J. S. Roberts, and A. C. Tropper, "10-GHz train of sub-500-fs optical soliton-like pulses from a surface-emitting semiconductor laser," IEEE Photon. Technol. Lett. **17**(2), 267–269 (2005).
9. A. H. Quarterman, K. G. Wilcox, V. Apostolopoulos, Z. Mihoubi, S. P. Elsmere, I. Farrer, D. A. Ritchie, and A. Tropper, "A passively mode-locked external-cavity semiconductor laser emitting 60-fs pulses," Nat. Photonics **3**(12), 729–731 (2009).
10. A. Tropper, and S. Hoogland, "Extended cavity surface-emitting semiconductor lasers," Prog. Quantum Electron. **30**(1), 1–43 (2006).
11. V. Baev, J. Eschner, E. Paeth, R. Schuler, and P. Toschek, ""Intracavity spectroscopy with diode-lasers," Appl. Phys," B-Photo **55**, 463–477 (1992).
12. V. Baev, T. Latz, and P. Toschek, "Laser intracavity absorption spectroscopy," Appl. Phys. B **69**(3), 171–202 (1999).
13. A. Garnache, A. A. Kachanov, F. Stoeckel, and R. Houdre, "Diode-pumped broadband vertical-external-cavity surface-emitting semiconductor laser applied to high-sensitivity intracavity absorption spectroscopy," J. Opt. Soc. Am. B **17**(9), 1589–1598 (2000).

#133908 - $15.00 USD Received 24 Aug 2010; accepted 16 Sep 2010; published 22 Sep 2010

14. A. Garnache, A. Ouvrard, and D. Romanini, "Single-Frequency operation of External-Cavity VCSELs: Non-linear multimode temporal dynamics and quantum limit," Opt. Express **15**(15), 9403–9417 (2007).
15. D. Findlay, and R. Clay, "The measurement of internal losses in 4-level lasers," Phys. Lett. **20**(3), 277–278 (1966).
16. M. Kuznetsov, F. Hakimi, R. Sprague, and A. Mooradian, "Design and characteristics of high-power (> 0.5-W CW) diode-pumped vertical-external-cavity surface-emitting semiconductor lasers with circular TEM00 beams," IEEE J. Sel. Top. Quantum Electron. **5**(3), 561–573 (1999).
17. A. Siegman, *Lasers,* (University Science Books, 1986) p. 359.

1. Introduction

In an optically-pumped quantum well vertical-external-cavity surface-emitting laser (VECSEL) [1] the gain is provided by a series of quantum wells positioned in the maxima of electric field intensity inside a microcavity, whose length is set to enhance either gain or bandwidth. Self-starting modelocking appears under the action of a semiconductor saturable absorber mirror, or SESAM [2]. The SESAM consists of a single quantum well, which contributes bleachable intracavity loss. The external cavity confers near-diffraction-limited beam quality, even with a large diameter active spot on the gain. Although femtosecond mode-locked VECSELs superficially resemble diode-pumped solid-state lasers in which an intra-cavity SESAM is used to initiate Kerr-lens or soliton modelocking, the mechanism by which they form ultrashort pulses is different. The optical path inside a VECSEL cavity contains at most a few μm length of material medium; thus the effect of self-phase-modulation and self-focussing is small, hence soliton or Kerr effects do not contribute to the pulse formation mechanisms [3]. Instead it is observed that a SESAM can have characteristics close to those of an ideal fast saturable absorber when used with broadband gain samples [4]. This is attributed to the quasi-instantaneous optical Stark effect, which is a fast, weak nonlinearity that broadens band-edge absorption resonances in the presence of an intense intracavity pulse [5,6]. The Stark effect was used in a VECSEL to generate sub-500-fs mode-locked pulses [7,8]. Since then, pulses with durations of 260 fs [7], 200 fs [3,7] and finally down to 60 fs [9] have been demonstrated in mode-locked VECSELs.

In fast saturable absorber mode-locking, the duration of the mode-locked pulse is determined by the competition between gain filtering which broadens the pulse and saturable absorption which shortens it. This is valid if we assume that group delay dispersion and self phase modulation are small. To achieve short pulses it is therefore essential to minimize the bandwidth-filtering effect of the gain structure so that the weak pulse shaping mechanism of the optical Stark effect can compete efficiently. The following factors combine to determine the gain spectrum of a surface-emitting quantum well structure: i) well thickness, composition of well and barriers; ii) number of wells, and their position in the active region; iii) carrier population in each well, trapped from the spatially inhomogeneous distribution created in the barriers by optical pumping; iv) temperature of the active region, and v) multilayer interference effects in the gain structure [2]. Thus, although the gain spectrum of a given well design can in principle be calculated [10], the compounded uncertainties of an as-grown structure allow at best an estimate of the likely gain bandwidth.

This paper describes an experimental determination of the gain filtering, *under continuous wave operating conditions*, of VECSEL gain structures designed for femtosecond laser operation. The method that we report here involves a spectro-temporal technique, derived from intra-cavity laser absorption spectroscopy (ICLAS) [11–14]. The transient evolution of the continuous wave (CW) laser spectrum is monitored and analyzed after the onset of lasing, in the approach to the steady state. The laser spectrum is initially broad: under the influence of gain filtering a process of spectral condensation occurs, during which the spectrum narrows and shifts to the peak of the gain profile. A master equation analysis of this process is described in Section 2. Section 3 describes the structures used for the experimental investigations. Section 4 presents the experimental data derived from gain structures which have yielded 500, 260 and 60-fs pulses in stable mode-locking using SESAMs with 0.3 and

#133908 - $15.00 USD Received 24 Aug 2010; accepted 16 Sep 2010; published 22 Sep 2010

0.6% modulation depths [6,7,9] and Section 5 discusses the measured gain filtering in the context of femtosecond mode-locked VECSELs.

2. Master equation analysis of spectral condensation

A typical VECSEL cavity with a longitudinal mode spacing of ~1 GHz, and total cavity losses of ~2% has a photon number decay rate, τ^{-1}, of ~3 × 10^6 s^{-1}, which is more than 100 times slower than the carrier decay rate of ~10^9 s^{-1}. The carrier population therefore follows the photon number adiabatically and relaxation oscillations are strongly damped. Therefore, the number of the laser equations is reduced from two to one; this is a "class A laser" and VECSEL is an excellent example of this type of laser dynamics. Within a few microseconds of the onset of lasing, both carrier population and total photon number have arrived close to their steady state values. The laser spectrum, however, can continue to change shape over a period of ~50 μs or more, during which the photon population is slowly redistributed over the cavity modes, out of the wings and into the centre, in response to the spectral curvature of the gain. This slow dynamic narrowing is referred to as spectral condensation in the ICLAS literature [12].

The physical properties of class A lasers simplify the analysis: we do not need coupled differential equations for photon number and carrier concentration. The time variation of the photon number, ϕ_q, in the q^{th} longitudinal mode, with angular frequency ω_q, is governed by the equation

$$\frac{d\phi_q}{dt} = -\frac{\phi_q}{\tau} + G_q(N)\phi_q, \tag{1}$$

where G_q is the modal gain per unit time in the q^{th} mode with a carrier density N [area^{-1}] in the active region. We assume that the modal gain varies linearly with N immediately around the operating point of the laser:

$$G_q(N) = (N - N_t)\gamma_q, \tag{2}$$

where γ_q are constants that characterize the modal gain spectrum. Spectral condensation continues after the total number of photons in the cavity summed over all modes has reached a constant equilibrium value:

$$\frac{d\Phi}{dt} = \sum_q \frac{d\phi_q}{dt} = 0. \tag{3}$$

In this regime the carrier density changes in response to changes in the photon spectrum, even though the number of photons is constant. Substitution of Eq. (2) in Eq. (1) and summation over q using also Eq. (3) yields

$$(N - N_t)\sum_q \gamma_q \phi_q = \frac{\Phi}{\tau}. \tag{4}$$

We can substitute for $(N - N_t)$ and get an equation that shows directly how the photon distribution changes in response to the cavity loss τ, and to gain, which amplifies some modes more than others:

$$\frac{d\phi_q}{dt} = -\frac{\phi_q}{\tau}\left(1 - \frac{\gamma_q}{\frac{1}{\Phi}\sum_q \gamma_q \phi_q}\right). \tag{5}$$

#133908 - $15.00 USD Received 24 Aug 2010; accepted 16 Sep 2010; published 22 Sep 2010

This master equation describes the evolution of a statistical distribution of photons. It is an integro-differential equation; the gain term feeding ϕ_q has a sum over the whole distribution in its denominator. Physically this means that the photon numbers in the different modes are coupled together by gain saturation; if there are a lot of photons in the cavity at one end of the spectrum, say, the other end of the spectrum sees less gain. The model does not take into account the effect of spontaneous emission, which adds photons randomly to the modes.

We are going to solve Eq. (5) to derive differential equations for the time variation of the moments of the photon distribution. We define the nth moment of the distribution, $\overline{\omega_n}$, like this:

$$\overline{\omega^n} = \frac{1}{\Phi}\sum_q \omega^n{}_q \phi_q. \tag{6}$$

The first moment, $\overline{\omega}$, defines the centre of the spectrum: the nth central moment of the distribution is defined by

$$\mu_n = \overline{(\omega - \overline{\omega})^n} = \sum_q (\omega - \overline{\omega})^n \phi_q. \tag{7}$$

Thus, $\mu_1 = 0$, and μ_2 is the variance of the spectrum, characterizing the square of its frequency bandwidth. We shall need the following relationships between moments and central moments:

$$\begin{aligned}
\overline{\omega^2} &= \mu_2 + \overline{\omega}^2, \\
\overline{\omega^3} &= \mu_3 + 3\mu_2\overline{\omega} + \overline{\omega}^3, \\
\overline{\omega^4} &= \mu_4 + 4\mu_3\overline{\omega} + 6\mu_2\overline{\omega}^2 + \overline{\omega}^4.
\end{aligned} \tag{8}$$

Since the spectral bandwidth of the laser shrinks rapidly to a value that is a small fraction of the gain bandwidth, it is reasonable to make a parabolic approximation for the gain spectrum, to simplify the model:

$$\gamma_q = \gamma_0\left(1 - \left(\frac{\omega_q - \omega_0}{\Omega_g}\right)^2\right), \tag{9}$$

where the gain peak is centered at the $q = 0$ mode with frequency ω_0, and has a frequency half-maximum half-width of Ω_g. When we substitute this form into Eq. (5), the factors of γ_0 cancel in the last term, and we obtain

$$\frac{d\phi_q}{dt} = -\frac{\phi_q}{\tau\Omega^2{}_g}\left(1 - \frac{1 - \left(\frac{\omega_q - \omega_0}{\Omega_g}\right)^2}{\frac{1}{\Phi}\sum_q\left(1 - \left(\frac{\omega_q - \omega_0}{\Omega_g}\right)^2\right)\phi_q}\right), \tag{10}$$

where the denominator can be written as

$$\frac{1}{\Phi}\sum_q\left(1 - \left(\frac{\omega_g - \omega_0}{\Omega_g}\right)^2\right)\phi_q = 1 - \left(\frac{\overline{(\omega - \omega_0)^2}}{\Omega^2{}_g}\right). \tag{11}$$

If we do a Taylor series expansion of the right-hand side of Eq. (10) we have

#133908 - $15.00 USD Received 24 Aug 2010; accepted 16 Sep 2010; published 22 Sep 2010

$$\frac{d\phi_q}{dt} = -\frac{\phi_q}{\tau\Omega_g^2}\left(\left(\omega_q - \omega_0\right)^2 - \overline{(\omega-\omega_0)^2}\right), \tag{12}$$

$$\overline{(\omega-\omega_0)^2} = \frac{1}{\Phi}\sum\left(\omega_q - \omega_0\right)^2\phi_q = \overline{\omega^2} - 2\omega_0\bar{\omega} + \omega^2{}_0. \tag{13}$$

We can use Eq. (13) in order to derive an equation for the time rate change of $\bar{\omega}$:

$$\begin{aligned}\frac{d}{dt}\bar{\omega} &= \sum_q \omega_q \frac{d\phi_q}{dt} = -\sum_q\left[\frac{\phi_q\omega_q}{\tau\Omega_g}\left(\left(\omega_q-\omega_0\right)^2 - \overline{(\omega-\omega_0)^2}\right)\right] \\ &= \frac{1}{\tau\Omega_g}\left(\overline{\omega\left(\omega_q-\omega_0\right)^2} - \bar{\omega}\overline{(\omega-\omega_0)^2}\right).\end{aligned} \tag{14}$$

If we expand the brackets under the overline, and then express the resulting moments as central moments, using the relationships in Eqs. (8) we derive this equation in a more useful form:

$$\frac{d\bar{\omega}}{dt} = -\frac{1}{\tau\Omega_g^2}\left(\mu_3 + 2\mu_2(\bar{\omega}-\omega_0)\right). \tag{15}$$

We can derive an equation for the time rate of change of the variance, μ_2, by expanding the brackets and expressing the resulting moments as central moments

$$\frac{d\mu_2}{dt} = -\frac{2\mu_2^2}{\tau\Omega_g^2}\left[\mu_4 + 2\mu_3(\bar{\omega}-\omega_0) - \mu_2^2\right]. \tag{16}$$

We approximate the spectrum of a VECSEL to be a smooth symmetrical Gaussian distribution, which has the form,

$$\Phi = \exp\left(-A(\omega-B)^2\right). \tag{17}$$

For the Gaussian distribution the central moments satisfy the recurrence relation, $\mu_n = (n-1)\mu_2\mu_{n-2}$. Given that the distribution is symmetrical, and only even central moments are non-zero we can rewrite Eq. (15) and Eq. (16) as

$$\frac{d\bar{\omega}}{dt} = -\frac{1}{\tau\Omega_g^2}2\mu_2(\bar{\omega}-\omega_0), \tag{18}$$

$$\frac{d\mu_2}{dt} = -\frac{2\mu_2^2}{\tau\Omega_g^2}. \tag{19}$$

In order to solve we substitute with $A = 1/2\mu_2$, whence

$$\frac{dA}{dt} = -\frac{1}{2\mu_2^2}\frac{d\mu_2}{dt} = \frac{1}{\tau\Omega_g^2}. \tag{20}$$

Experimentally we measure the optical spectrum of the laser at various times *t* after the onset of lasing, and calculate the value of μ_2, and hence *A* for each time *t*. If the model assumptions are valid for the experimental laser, then a graph of *A* versus *t* shows a linear relationship, from which we extract *dA/dt*. We take a value for the cavity lifetime, τ, determined experimentally by the method of Findlay and Clay described in Section 4, and deduce the effective half-width half-maximum gain bandwidth, Ω_g, by simply rearranging Eq. (20):

#133908 - $15.00 USD Received 24 Aug 2010; accepted 16 Sep 2010; published 22 Sep 2010

$$\Omega_g = \sqrt{\frac{1}{\tau \frac{dA}{dt}}}. \tag{21}$$

3. Description of gain structures

We experimentally determine the gain dispersion of two samples. The first is a 6-quantum well (QW) structure grown by MOCVD (QT1544), which has been used to demonstrate first 500 and then 260-fs mode-locked pulses using two different SESAMs, one having twice the modulation depth of the other [6,7]. The gain sample acts as a turning mirror in a typical VECSEL cavity, so the bottom stack is composed of an AlAs/GaAs Bragg structure with a calculated reflectivity of 99.95% at the 1030 nm design wavelength. The active region consists of 6 compressively strained 8-nm $In_{0.23}Ga_{0.77}As$ quantum wells designed for peak room-temperature photoluminescence at 1025 nm. Barriers of $GaAs_{0.94}P_{0.06}$ either side of each well strain-balance the active region, and GaAs spacer layers are used to position the wells at successive maxima of the intracavity standing wave energy in the 7λ/2 active region in a 2-1-1-1-0-1 arrangement, as can be seen in the simulation of the electric field shown in Fig. 1. The arrangement is chosen to provide a homogeneous excitation of the QWs under optical pumping. The top confinement layer consists of a quarter wavelength AlAs layer with an 8 nm GaAs capping layer grown on the top. The active region absorbs 50% of the incident pump power, generating carriers, which are then trapped by the InGaAs quantum wells to provide gain near 1040 nm. The total optical thickness between the top Bragg layer and the air interface is chosen to create a structure, which is almost anti-resonant, thus, spectrally broad.

The second gain sample was grown using molecular beam epitaxy (A4226). Like QT1544 it has a 7λ/2 active region with the same arrangement of wells, but there are no strain balancing layers, so the barriers are of GaAs. The crucial difference in the design of A4226 is that the thickness of the top confinement layer is defined so that the structure lases exactly at the anti-resonant wavelength of the optical microcavity formed between the DBR and the air interface, increasing the effective gain bandwidth relative to earlier structures. A4226 is the gain sample used in [9] for the generation of 60 fs pulses, using the SESAM that generated 260-fs pulses with QT1544 [7].

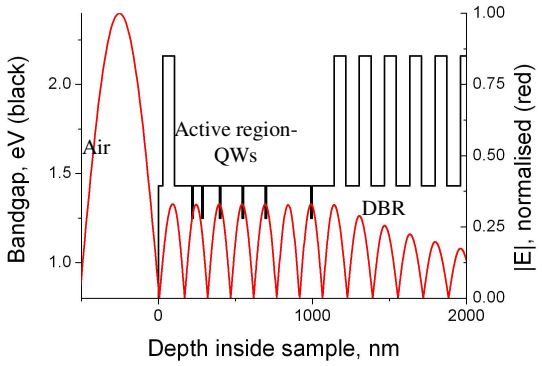

Fig. 1. The electric field inside the microcavity of the A4226 gain sample. The quantum wells are positioned in the maxima of the modulus of the electric field.

4. Spectrotemporal measurements of VECSELs

Figure 2 shows a schematic drawing of the experimental setup used. The CW VECSEL was optically pumped using an 830 nm, 1.3 W diode laser. The cavity of the VECSEL had a W shape with a round trip time of 3 ns. M1, M2 and M3 were high reflectors (HR) with radius of

#133908 - $15.00 USD Received 24 Aug 2010; accepted 16 Sep 2010; published 22 Sep 2010

curvature −100 mm, −38 mm and plane respectively. The output coupler (OC) had a radius of curvature −50 mm.

The loss l_i of each cavity from sources other than output coupling was determined by measuring threshold pump power, P_{th}, as a function of output coupling, using output couplers with loss l_{OC} values of 5×10^{-4}, 3×10^{-3}, and 7×10^{-3}. In the standard Findlay-Clay analysis for a 4-level laser, P_{th} is assumed to be linearly proportional to total cavity loss, $l_{OC} + l_i$, and thus the intercept of the P_{th} versus l_i line on the $P_{th} = 0$ axis corresponds to $-l_i$ [15]. This analysis must be modified for a semiconductor laser, in which the unsaturated gain coefficient, g, is a nonlinear function of pump power. We represent this nonlinear dependence using the empirical function $g = g_0 \ln\left(P/P_0\right)$, where g_0, which scales the overall gain, is proportional to the number of quantum wells, and P_0 is the pump power required to make the gain structure transparent. The Findlay-Clay plot then takes the form $P_{th} = P_0 \exp\left[\left(l_{OC} + l_i\right)/g_0\right]$. The exponential is indistinguishable from a straight line for the small arguments that we use experimentally; however the intercept on the $P_{th} = 0$ axis now corresponds to $-\left(l_i + g_0\right)$. We follow Kuznetsov et al. [16], who modelled the performance of a VECSEL based on strained 8-nm $In_{0.16}Ga_{0.84}As$ wells, in estimating a value for g_0 based on a gain coefficient of 2000 cm^{-1}: for 6 8-nm wells this predicts $g_0 = 9.6 \times 10^{-3}$. The results of the modified Findlay-Clay characterisation are summarised in Table 1. Changing between the two wafers the cavity was rebuilt. As the A4226 and QT1544 wafers have equally good surface under microscope inspection we believe that the reason for the larger value of l_i measured in the A4226 cavity is due to the presence of lattice defects in this non-strain-compensated sample.

Table 1. Values for the loss analysis for samples QT1544 and A4226

	F-C intercept	error	l_i	roundtrip time (ns)	total loss	photon lifetime (ns)
QT1544	0.0181	0.0005	0.0085	2.973	0.0115	259 ± 10
A4226	0.029	0.001	0.02	2.973	0.0233	127 ± 8

The spectro-temporal measurements were performed using an OC transmission of 0.3%. The laser cavity mode was modulated using a mechanical chopper at 400 Hz taking care not to modulate the optical pump so that the thermal load in the gain structure stays approximately constant. The gain structure was kept at a heat sink temperature of 10 °C by a thermoelectric element.

#133908 - $15.00 USD Received 24 Aug 2010; accepted 16 Sep 2010; published 22 Sep 2010

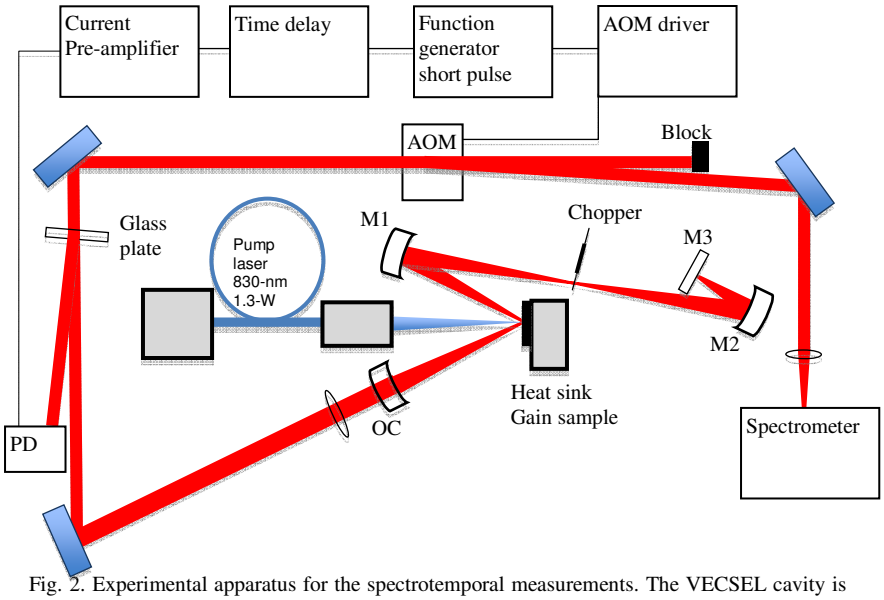

Fig. 2. Experimental apparatus for the spectrotemporal measurements. The VECSEL cavity is formed between mirrors M1, M2, M3, the gain sample and the output coupler, OC.

To record the optical spectra at different generation times a small fraction of the modulated laser output was detected by the photodiode and used to trigger the first function generator. This function generator was used to produce a variable delay, triggering the second function generator, which produced a single pulse lasting 3μs. This was used to drive the acousto-optic modulator (AOM). The AOM deflected the output of the VECSEL providing a short, controllable delay before the time window in which the laser light was detected by the spectrometer. Spectra were recorded every 3.75 μs from initial laser onset until the spectrum finished condensing for gain samples QT1544 and A4226. The recorded spectra for delays between 18.75 and 45 μs are shown in Fig. 3 for QT1544. In Fig. 3 the spectra are seen for a pump power of 1.2 W, the measurement was repeated for three different pump powers of 1.1, 1.2 and 1.3W. The small periodic ripples that can be observed on the spectra are caused by the gain sample substrate acting as an etalon. This etalon effect could be removed by polishing the substrate at an angle, however in this case the effect is relatively weak and does not affect our results.

#133908 - $15.00 USD Received 24 Aug 2010; accepted 16 Sep 2010; published 22 Sep 2010

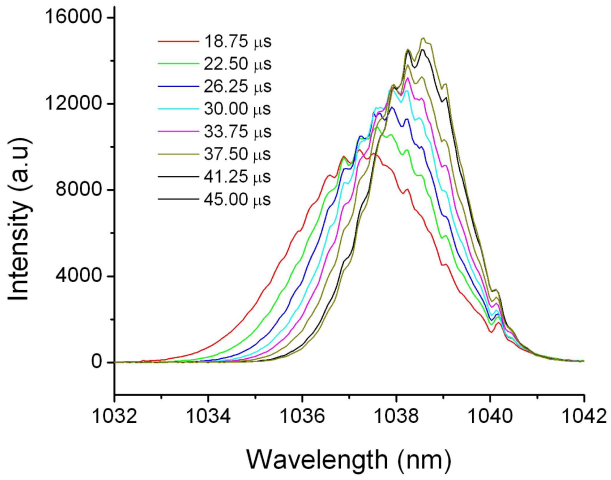

Fig. 3. Spectra acquired from gain sample QT1544 in a range of time intervals from 18.75 to 45.00 μs, for a pump power of 1.2 W. The ripples in the spectra are due to modulations of the cavity formed between the back surface of the gain chip and the DBR.

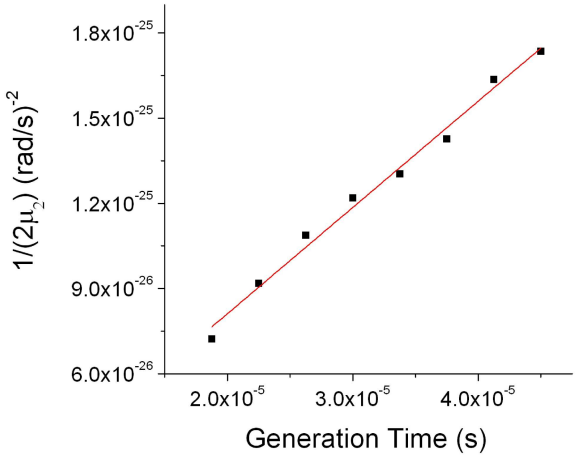

Fig. 4. Evolution of $A = 1/2\mu_2$ with generation time for sample QT1544 corresponding to the graph depicted in Fig. 3. The slope of the fit is 3.74×10^{-21} s/rad^2.

The spectra were analysed to find the second central moment μ_2, for each spectrum recorded. Due to the fact that spectra at early times condensed quickly and they were very broad with a poor signal to noise, only latter times were used in order to minimize jitter error. The measurements for μ_2, were then plotted as *1/2* μ_2 versus generation time, shown in Fig. 4. Figure 4 shows a linear dependence on *1/2* μ_2 as expected from the theory.

The recorded spectra for delays between 18.75 and 45 μs are shown in Fig. 5 also for A4226 at a pump power of 1.2 W. Again, the measurement was repeated for three different pump powers of 1.1, 1.2 and 1.3 W. In Fig. 6 the graph of *1/2* μ_2 versus generation time can be seen and again it shows a linear dependence on *1/2* μ_2 as expected from the theory.

#133908 - $15.00 USD Received 24 Aug 2010; accepted 16 Sep 2010; published 22 Sep 2010

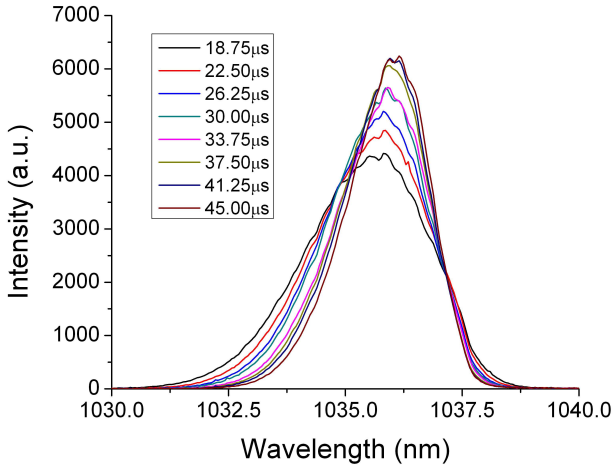

Fig. 5. Spectra acquired from gain sample A4226 in a range of time intervals from 18.75 to 45.00 μs, for a pump power of 1.2 W.

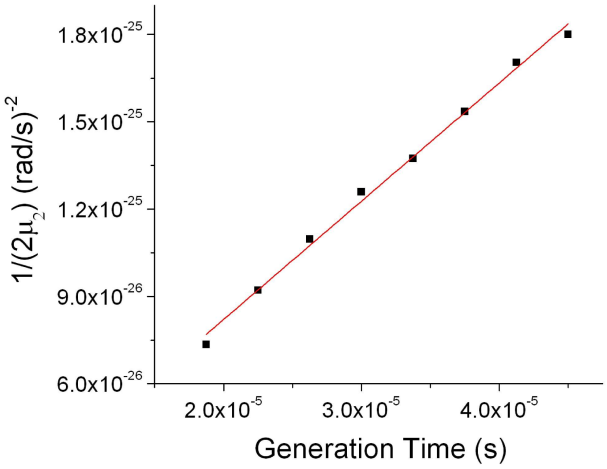

Fig. 6. Corresponding graph to the graph of Fig. 5 which shows the evolution of $A = 1/2\mu_2$ with generation time for sample A4226. The slope of the fit is 4.06x10^{-21}s/rad^2.

Using the gradient of the fitted slopes, along with the calculated photon cavity lifetimes for the two gains, the effective gain bandwidth can be calculated using Eq. (21). We calculate the effective gain bandwidth to be 37 ± 7 nm FWHM for QT1544 and 51 ± 13 nm for A4226. The measurements were obtained by averaging our results for the three different pump powers. The detailed results for the different pump powers can be seen in Table 2 and Table 3 for QT1544 and A4226 respectively.

Table 2. QT1544 bandwidth for different pump powers

Pump power (W)	Central Wavelength (nm)	Bandwidth (nm)
1.1	1037.6	34.0
1.2	1038.5	37.3
1.3	1039.2	39.4

#133908 - $15.00 USD Received 24 Aug 2010; accepted 16 Sep 2010; published 22 Sep 2010

Table 3. A4226 bandwidth for different pump powers

Pump power (W)	Central Wavelength (nm)	Bandwidth (nm)
1.1	1035.6	51.0
1.2	1036.0	52.8
1.3	1036.1	49.8

It is important to note that the effective bandwidth values in Tables 2 and 3 represent a measure of the curvature of the gain profile around the laser operating wavelength; they are not the same as the FWHM value of the gain profile, which is not parabolic overall. However, it is the curvature of the gain profile, and not the actual gain bandwidth, that is the physical quantity directly responsible for filtering and stretching short pulses.

5. Discussion in relation to femtosecond mode-locked VECSELs

The gain filter bandwidth calculated gives us the curvature of the gain curve, which corresponds to a pulse lengthening mechanism. One can estimate the increase in pulse duration per roundtrip, Δt_p, caused by this gain curvature, which is dependant on the bandwidth and the estimated gain of the cavities, following reference [17]. For both gain samples the pulse lengthening per roundtrip for a pulse width, t_p = 500 fs is of the order of $6x10^{-5}t_p$.

The equivalent group delay dispersion that would cause this pulse lengthening effect is calculated to be 2700 fs^2. Group delay dispersion caused from the materials is small as the pulse travels not more than some tens of microns in the gain and saturable absorber mirror samples; group delay dispersion due to multilayer effects can be estimated and minimized by design. The theoretical group delay dispersion of our gain and absorber samples is estimated to be some hundreds of fs^2 per roundtrip including the contributions of materials and of the structure. Therefore, the estimated value of 2700 fs^2 confirms our expectation that gain dispersion is the dominant pulse lengthening effect in our lasers. This means that at steady state in a mode-locked laser the pulse lengthening mechanism calculated here will be balanced by the pulse shortening mechanism of the saturable absorber mirror. The optical Stark effect has been suggested as the mode-locking mechanism responsible for femtosecond pulse generation in mode-locked VECSELs. We have shown that this effect assuming no bleaching of a saturable absorber produces a pulse shortening per roundtrip of order $10^{-4}t_p$ for t_p = 500 fs [5]. This estimated value of pulse shortening is of similar magnitude to the pulse lengthening effect of the gain estimated here, and hence is indicative that the optical Stark effect could be the dominant pulse shortening mechanism.

In [8] we reported 477 fs pulse duration using a SESAM with modulation depth 0.3%. By doubling the modulation depth of the SESAM the pulse duration was reduced to 260 fs [7]. This is consistent with the fast saturable absorber mode-locking model, where the balance of gain dispersion and pulse shortening set the steady state pulse duration [4].

The A4226 gain structure in [9] has a pure antiresonant design using the same SESAM as [7] and demonstrated 60 fs pulses. This gain structure has a gain bandwidth measured here to be 51 nm, in comparison to 37 nm of QT1544. An antiresonant design is preferable for the generation of shorter pulses as the flatter gain curve should increase the pulse width less per round trip and thus permit the saturable absorber to further decrease the pulse width. However, here, due to A4226 exhibiting more loss per round trip than QT1544 the resulting pulse width increase we estimate is similar in both samples. It is clear though that the operation of this laser [9] is quite difficult to interpret; the 60 fs pulse duration is close to carrier-carrier scattering times and spectral hole burning is also affecting the laser operation.

We can conclude that gain filtering crucially affects the femtosecond pulse characteristics, we are not limited by gain bandwidth or GDD but by the interplay of gain curvature with the pulse shortening mechanism provided by the SESAM. However, reducing the gain dispersion further may not simply lead to shorter pulses: as pulse durations approach carrier-carrier

#133908 - $15.00 USD Received 24 Aug 2010; accepted 16 Sep 2010; published 22 Sep 2010

scattering timescales other phenomena, such as spectral hole burning, begin to play a significant role in the pulse shaping [9].

6. Conclusions

We report a method for experimentally determining the gain filter of a CW VECSEL under operating conditions. A spectro-temporal technique, inspired from intra-cavity laser absorption spectroscopy (ICLAS) [11,12], is used. A master equation analysis of this process was described that is applicable to class A lasers. We experimentally measured the effective gain bandwidths of QT1544 [6,7] and A4226 [9], which have yielded femtosecond pulses when mode-locked with an optical Stark SESAM. The measured effective gain bandwidth is 37 ± 7 nm FWHM for QT1544 and 51 ± 13 nm for A4226.

This study confirms our sample design rules for the gain samples in VECSELs and helps us gain insight in their mode of operation. It shows that the pulse width is defined by the interplay of gain filtering and the pulse shortening, with group delay dispersion playing a minor role, and that minimising the curvature of the gain profile is of critical importance in designing gain samples for femtosecond mode-locked VECSELs.

#133908 - $15.00 USD Received 24 Aug 2010; accepted 16 Sep 2010; published 22 Sep 2010